NANO · MICRO small
www.small-journal.com

Systematic Investigation of Novel, Controlled Low-Temperature Sintering Processes for Inkjet Printed Silver Nanoparticle Ink

Zehua Chen, Ulrich Gengenbach, Liane Koker, Liyu Huang, Tim P. Mach, Klaus-Martin Reichert, Richard Thelen, and Martin Ungerer*

Functional inks enable manufacturing of flexible electronic devices by means of printing technology. Silver nanoparticle (Ag NP) ink is widely used for printing conductive components. A sintering process is required to obtain sufficient conductivity. Thermal sintering is the most commonly used method, but the heat must be carefully applied to avoid damaging low-temperature substrates such as polymer films. In this work, two alternative sintering methods, damp heat sintering and water sintering are systematically investigated for inkjet-printed Ag tracks on polymer substrates. Both methods allow sintering polyvinyl pyrrolidone (PVP) capped Ag NPs at 85°C. In this way, the resistance is significantly reduced to only 1.7 times that of the samples on polyimide sintered in an oven at 250°C. The microstructure of sintered Ag NPs is analyzed. Taking the states of the capping layer under different conditions into account, the explanation of the sintering mechanism of Ag NPs at low temperatures is presented. Overall, both damp heat sintering and water sintering are viable options for achieving high conductivity of printed Ag tracks. They can broaden the range of substrates available for flexible electronic device fabrication while mitigating substrate damage risks. The choice between them depends on the specific application and the substrate used.

1. Introduction

With the emergence of functional inks, printing technologies can be applied to manufacture various flexible electronic devices, such as sensors,[1,2] photovoltaic cells,[3,4] organic light-emitting diodes (OLED)[5,6] or wearable devices.[7] Silver nanoparticle (Ag NP) ink is often utilized for printing electrodes, circuits,[8,9] antennas for radio frequency identification (RFID),[10] and other conductive components. Ag NP ink consists of dispersions of Ag NPs, coated with capping agents to avoid agglomeration in the surrounding organic solvents.[11] The viscosity of the ink is adjusted to suit different printing techniques, such as inkjet printing and screen printing. After printing, due to the presence of solvents and capping agents around the Ag NPs, the printed pattern usually has a very high resistance or no conductivity at all. Hence, to obtain good conductivity, the printed pattern needs to be dried and sintered to remove the solvents and capping agents, allowing the Ag NPs to aggregate or make contact to form effective conductive paths.

Various sintering approaches for Ag NP have been reported in the literature.[12,13] The most commonly used method is thermal sintering.[14,15] The substrate with the printed pattern is placed in an oven at a certain temperature for a certain time. Due to their larger surface-to-volume ratio, Ag NPs show a melting point depression compared to bulk Ag.[16] Thus, Ag NPs require a lower sintering temperature. Chou et al. found that noticeable sintering of Ag NP (the average size of the Ag NPs is about 46nm) starts at about 100°C and the corresponding generated Ag film exhibits the best conductivity after sintering at 250°C.[14] Heat can also be locally applied by infra-red (IR) radiation,[17] intense pulsed light (IPL),[18,19] laser light,[20–25] by resistive heating with direct current (DC)[26] or alternating current (AC),[27] and with microwaves.[28] For flexible printed electronics, the most commonly used substrates are polymer films, such as polyethylene terephthalate (PET), polyethylene naphthalate (PEN), and polyimide (PI).[29] Except for more expensive high-temperature substrates such as PI films, processing of most polymer films is

Z. Chen, U. Gengenbach, L. Koker, L. Huang, K.-M. Reichert, M. Ungerer
Institute for Automation and Applied Informatics
Karlsruhe Institute of Technology
76344 Eggenstein-Leopoldshafen, Germany
E-mail: zehua.chen@kit.edu
T. P. Mach
Institute for Applied Materials - Energy Storage Systems
Karlsruhe Institute of Technology
76344 Eggenstein-Leopoldshafen, Germany
R. Thelen
Institute of Microstructure Technology
Karlsruhe Institute of Technology
76344 Eggenstein-Leopoldshafen, Germany

The ORCID identification number(s) for the author(s) of this article can be found under https://doi.org/10.1002/smll.202306865

DOI: 10.1002/smll.202306865

usually carried out at temperatures between 120 and 180°C.[30] Thus, the process parameters of heat-assisted sintering methods must be carefully adjusted to avoid substrate damage. As a result, finding ways to sinter Ag NP ink structures at low temperatures without substrate damage has become an important research field.

The solution-assisted chemical sintering method promises low-temperature alternatives for sintering Ag NPs. Magdassi et al. introduce a novel approach that triggers the spontaneous 3D coalescence of Ag NPs using a cationic polymer, poly(diallyldimethylammonium chloride) (PDAC) solution at room temperature (RT). The silver patterns are printed on the copier paper pre-coated by the PDAC solution. Silver particles within the patterns are spontaneously sintered at RT, having a sheet resistance of 0.68Ωsq^{-1} and a resistivity of 70 μΩcm.[31] Tang et al. achieve a resistivity of 9.91 μΩcm (about 16% of the bulk Ag) by placing printed Ag patterns in saturated sodium chloride solution for 70 min at RT.[32] Corsino and Balela utilize 50mM sodium chloride aqueous solution as the solvent of an Ag NP ink, and this ink with 15wt.% Ag exhibits a sheet resistance of about 2.85Ωsq^{-1}.[33] Peng et al. soak printed Ag NP tracks in potassium chloride solution at RT, reducing the resistance of the Ag track by eight orders of magnitude.[34] Xiao et al. spray a sodium hydroxide solution on the Ag NP patterns on PET at RT, achieving a resistivity of 12.11 μΩcm.[35] Olkkonen et al. immerse the Ag tracks in boiling salt water (110°C) for 20 min, and the silver tracks exhibit a resistivity of about 3.18 μΩcm.[36] The aforementioned approaches use ion solutions as destabilizing agents to remove the capping agents around the Ag NPs. After the destabilization process, coalescence, and Ostwald ripening of the Ag NPs occur, yielding neck formation between the Ag NPs thus improving the conductivity of the printed structures.[13,37,38] However, the ion solution needs to be subsequently washed away,[32,36] requiring an additional step, which can weaken the adhesion between the printed Ag layer and the substrate further.

Pure water or high humidity are also found beneficial for the sintering effect. Olkkonen et al. find that a significant enhancement in conductivity can be obtained with pure boiling water treatment.[36] Allen et al. obtain the resistivity of printed Ag patterns of 5.88 μΩcm by exposing substrates with ink-receptive coatings to 85% relative humidity (RH) at RT before and after printing.[39] Bourassa et al. observe the influence of humidity on Ag NP sintering qualitatively by putting a cup of water (10g) in a bottom tray in the oven at 120°C for 60 min, resulting in a resistivity of 3.24 μΩcm.[38] They raise the assumption that the observed sintering effect is due to water influence on the capping layer and sintering pressure on the NPs due to the water surface tension.

In the present work, to our best knowledge, we are the first to systematically investigate the influence of water and humidity on the sintering effect for inkjet printed Ag NPs under controlled conditions by applying two sintering methods, controlled damp heat sintering and water sintering. The printed Ag tracks (ink: Silverjet DGP 40LT-15C) on various polymer substrates (PET NB-TP-3GU100, PET Melinex ST506, and PI Kapton HN) are subjected to either 85%RH in a climate chamber or to immersion in deionized water (DIW) at three different temperatures, respectively. Both processes allow Ag NPs to sinter at a comparably low temperature of 85°C, resulting in a significant reduction in resistance. Additionally, the influence of two drying methods (vacuum and thermal drying) on the resistivity of the printed structures before water sintering is explored. The resulting microstructure of sintered Ag NPs is characterized by scanning electron microscopy (SEM) imaging and atomic force microscopy (AFM) imaging. Based on our investigations, we substantiate the above-mentioned assumption of Bourassa et al.[38] Taking the states of the capping layer under different conditions into account, we systematically explain the sintering mechanism of Ag NPs at low temperature ranges.

2. Results and Discussion

This section is divided into five subsections including the results of inkjet printing, damp heat sintering, and water sintering, as well as the influences of drying processes for ink solvent removal on the water sintering effects. Furthermore, a discussion of the obtained results is presented.

2.1. Inkjet Printing

The printed Ag tracks on NB-TP-3GU100 substrates exhibit notable differences from those printed on Melinex ST506 and Kapton HN substrates. Due to different substrate wetting properties, the Ag tracks on NB-TP-3GU100 substrates show significantly lower widths than those on Melinex ST506 and Kapton HN substrates (**Figure 1**). The measured mean width and profile area of Ag tracks are 122.13(6.91)μm and 149.27(20.20)μm^{-2} on NB-TP-3GU100, 229.13(9.55)μm and 127.00(7.96)μm^{-2} on Melinex ST506, and 222.6(12.82)μm and 131.6(10.61)μm^{-2} Kapton HN substrates, respectively (Figure S2, Supporting Information).

2.2. Damp Heat Sintering Results

A high humidity environment has a positive effect on sintering. As shown in **Figure 2**, similar tendencies can be observed in the samples printed on three types of substrates. Under constant humidity of 85% RH, the resistance is further reduced when higher temperatures are applied. The resistance drops sharply within the first hour of damp heat sintering. Without a high humidity environment, there is a lower sintering effect. The resistance of reference samples on NB-TP-3GU100 sintered in the oven at 85°C after 24 h is reduced only by 12%, while the resistance of the samples sintered in the climate chamber at 85°C and 85%RH is reduced by 69%. Unlike NB-TP-3GU100 substrates, at 23°C and 85%RH, hardly any sintering effect is observed on Melinex ST506 substrates (cf. Figure 2a, 2b). This difference can be also attributed to the water adsorption ability of substrates. The roughness of the NB-TP-3GU100 substrate is greater than that of the Melinex ST506 substrate (Table S1, Supporting Information). The NB-TP-3GU100 substrates have an about 38μm thick porous coating[40] on the surface, which can adsorb more water moisture. This may promote neck formation between Ag NPs, leading to better conductivity already at a low temperature. The surface of Melinex ST506 substrates is smoother and less prone to water adsorption, thus less prone to neck formation between Ag NPs at low temperatures. On the other hand, due

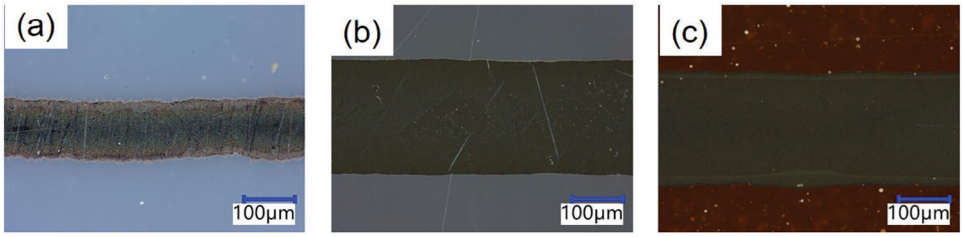

Figure 1. Inkjet printed Ag tracks on a) NB-TP-3GU100, b) Melinex ST506, and c) Kapton HN substrates.

to the nanoporous coating, NB-TP-3GU100 substrates are thermally more sensitive in dry state. They are slightly bent after sintering in the oven already at 85°C while this effect is not observed in the climate chamber for 85°C and 85%RH. This small deformation may put mechanical stress on the printed tracks and lead to poor conductivity. Melinex ST506 substrates are capable to withstand temperatures up to 150°C. No deformation is observed when holding them in the oven at 85°C. Figure 2c demonstrates the effectiveness of damp heat sintering (85°C and 85%RH) on printed Ag tracks on Kapton HN substrates. Before sintering, the resistance of printed samples on Kapton HN substrates is 66.00(1.47)Ω. After one hour of damp heat sintering, the resistance reduces to 23.38(0.40)Ω. The resistance is about only twice that of the samples thermally sintered at 250°C for one hour 10.65(1.03)Ω. After 24 h of damp heat sintering, the resistance reduces to 17.66(0.58)Ω (the calculated resistivity is 5.16µΩcm, Table S4, Supporting Information), which is only 1.7 times that of the sample thermally sintered at 250°C for 24 h (10.58(0.13)Ω, with the calculated resistivity of 3.09µΩcm).

The SEM images in **Figure 3** provide morphological evidence that supports the obtained resistivity data in Figure 2. Sintering Ag NPs in a high humidity environment (85%RH), even at a low temperature below 100°C, can result in noticeable particle necking and formation of a porous, mesh-like network structure, without significant growth of Ag NPs on PET films. It can be observed that the higher temperatures result in more neck formation between Ag NPs, leading to lower resistance. Furthermore, it provides evidence that the presence of water moisture is crucial

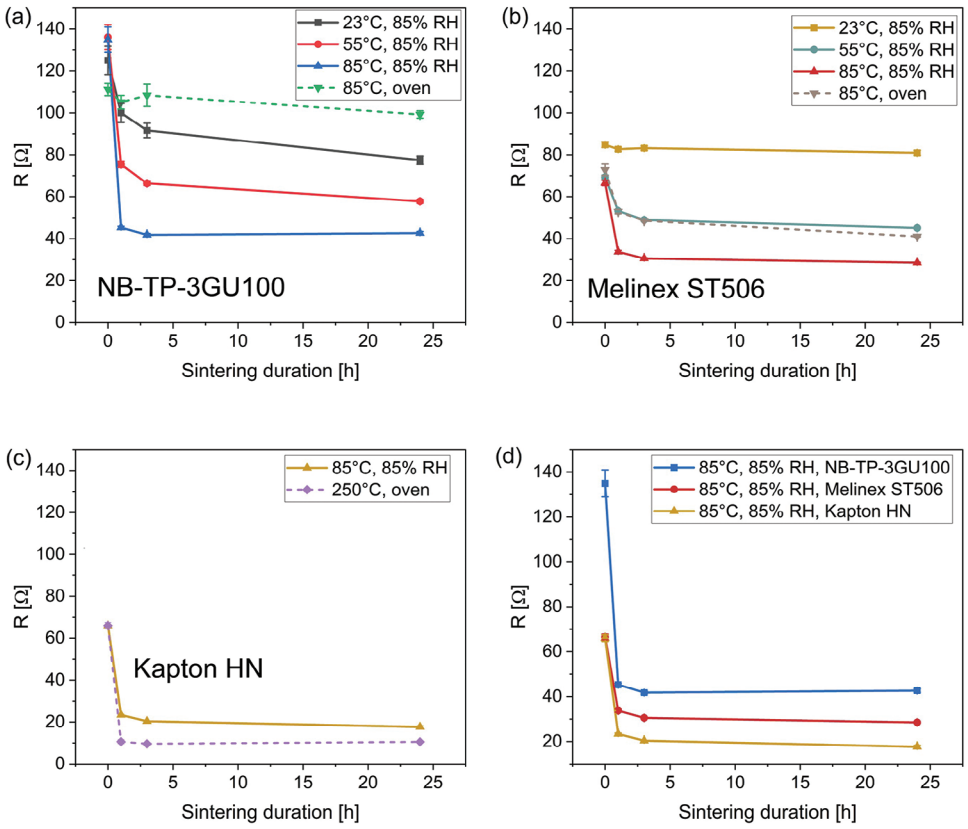

Figure 2. The effect of damp heat sintering on printed Ag tracks is investigated on a) NB-TP-3GU100, b) Melinex ST506, and c) Kapton HN substrates under different sintering conditions. d) Comparison of the damp heat sintering effect (85°C, 85%RH) between printed samples on NB-TP-3GU100, Melinex ST506, and Kapton HN substrates. Three to five printed samples are analyzed for each condition. The resistances (R) of printed Ag tracks are measured after one hour, three hours, and 24 h of sintering. Error bars represent standard deviations.

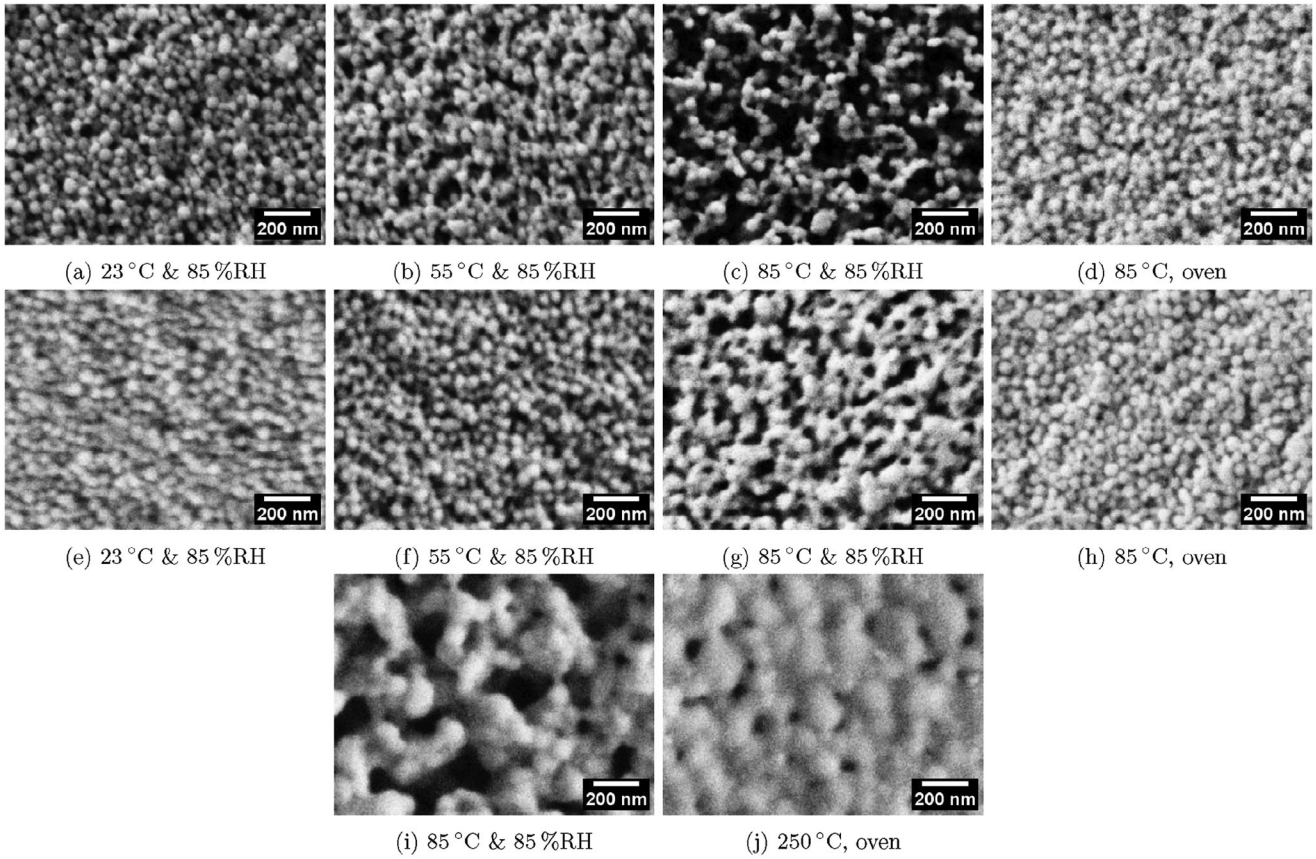

Figure 3. SEM images of Ag NPs on different substrates after sintering under different conditions. All images have the same magnification. a–d): Ag NPs on NB-TP-3GU100 substrates sintered in a climate chamber under damp heat conditions for 24 h. e–h): Ag NPs on Melinex ST506 substrates sintered in a climate chamber under damp heat conditions for 24 h. i–j): Ag NPs on Kapton HN substrates sintered in a climate chamber (i) and in an oven (j) for 24 h.

in forming necks between Ag NPs. Finally, on Kapton HN substrates, Figure 3i,j shows a structural difference between damp heat (85°C, 85%RH) and oven (250°C) sintered Ag NPs. Under the damp heat condition, more neck formation between Ag NPs is observed, while at 250°C in the oven, stronger growth of the Ag NPs occurs.

2.3. Water Sintering Results

The resistances before and after water sintering of samples printed on three types of substrates with different water sintering durations are depicted in **Figure 4**. The presence of liquid water has a more pronounced effect on sintering. The best sintering effect occurs when the temperature of DIW is raised to 85°C. Among all the three types of substrates, a sharp reduction in resistance occurs within the first minute of immersion (the resistance drops by 60% on NB-TP-3GU100, 51% on Melinex ST506 and 67% on Kapton HN.)

To discriminate the influence of fluid heat transfer from the supposed influence of water on the capping agents, both printed Ag tracks on NB-TP-3GU100 and Melinex ST506 substrates are immersed in silicone oil at 85°C. For both substrates, after 64 min of immersion in 85°C of silicone oil, the changes in resistance are much less than those immersed in 85°C of DIW (see Figure 4a,b), providing evidence that, compared to heat transfer, the influence of water dominates the sintering effect.

Figure 4d shows the comparison of water sintering effect for the printed Ag tracks on three types of substrates. Similar to damp heat sintering, water sintering is most effective for Ag tracks on Kapton HN substrates. However, as shown in **Figure 5**, the adhesion between printed Ag tracks and Kapton HN substrate is very weak, with the printed Ag tracks peeling off the substrate after four minutes of immersion. Nevertheless, the samples remain on the Kapton HN substrate when there is only one minute of immersion, and the resistance 28(0.57)Ω is only about twice that of samples sintered in an oven at 250°C for one minute 13.38(0.44)Ω. The fact that the printed tracks and pads detach sectionally while keeping their initial shape demonstrates that the cohesion among the particles is significantly stronger than the adhesion to the substrate, substantiating the assumption of a noticeable sintering level.

Figure 6 presents the SEM images of the surface morphology of the water sintered Ag NPs. Similar to damp heat sintering, a porous, mesh-like structure of Ag NPs can be observed after sintering in DIW. Furthermore, the higher the temperature of the DIW, the faster and more pronounced the formation of this network. Figure 6d,h show the SEM images of Ag NPs sintered

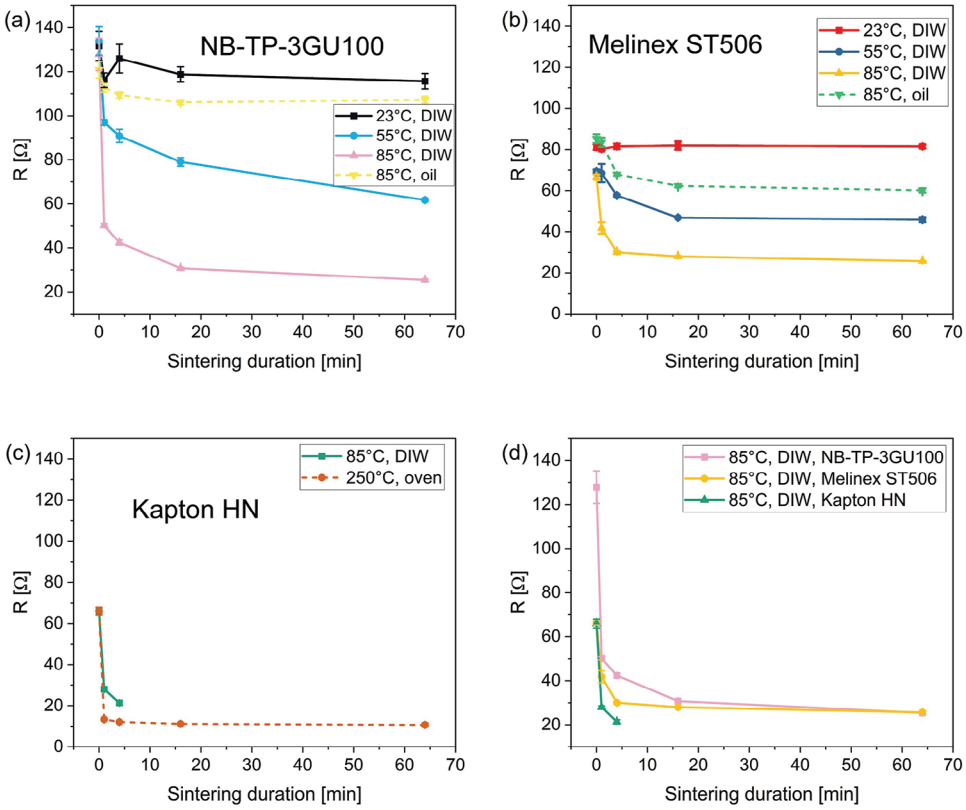

Figure 4. The effect of water sintering and immersion in silicone oil on printed Ag tracks on a) NB-TP-3GU100, b) Melinex ST506, and c) Kapton HN substrates at different temperatures. d) Comparison of the water sintering effect (85°C of DIW) between printed samples on three types of substrates. The sintering durations are set to 0 min (unsintered samples), 1, 4, 16, and 64 min. For each sintering duration, five printed samples are characterized. The resistances are measured before and after immersing the samples in DIW/oil. R represents the resistance of the Ag tracks after each immersion in DIW/oil. Error bars represent standard deviations.

in an oil bath at 85°C for 64 min, and there is no obvious neck formation, indicating that water facilitates the neck formation, yielding more conductive paths that improve high conductivity.

2.4. Influence of Drying Processes for Ink Solvent Removal on the Water Sintering Effect

Before water sintering, the printed Ag tracks need to be dried to avoid damage in water. In this work, the potential influence of two drying processes on the final water sintering effect is investigated. Section 2.3 reveals that a duration of 16 min is sufficient for a significant reduction of resistance by water sintering of Ag NP tracks on Melinex ST506. Hence, this process is used as a baseline to examine the influence of drying processes for ink solvent removal on water sintering.

2.4.1. Vacuum Drying

As the temperature of the substrate plays also a role in removing ink solvent during printing, samples are printed on Melinex ST506 substrates at three different temperatures (23, 55, and 85°C) and then subjected to vacuum drying for 40 min. As shown in **Table 1**, the samples printed at 23 or 55°C and vacuum dried remain non-conductive even after three days of storing under room conditions, whereas the samples without vacuum dried become conductive (399.67 and 178.60Ω, respectively). The samples printed at 23 and 55°C, undergoing vacuum drying and subsequent 16 min of water sintering at 85°C yield resistances of 180.63 and 49.86Ω, respectively. The results indicate that the neck formation of Ag NPs, which leads to high conductivity of the printed tracks, is hindered by vacuum drying. In the dry state, the ambient environment cannot promote neck formation between

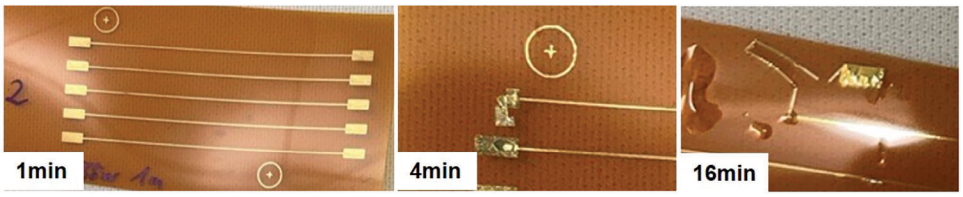

Figure 5. Samples on Kapton HN substrates after immersing into DIW at 85°C for different durations.

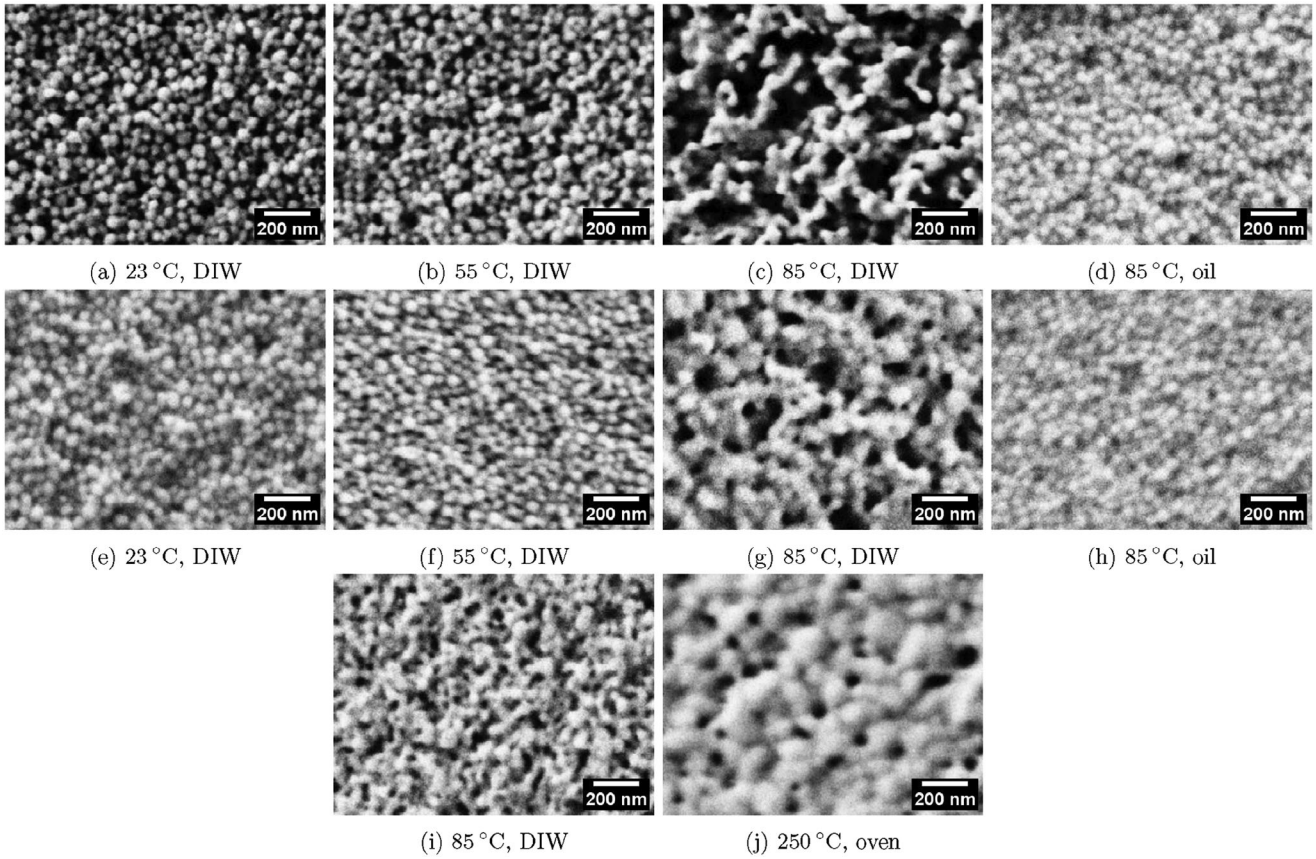

Figure 6. SEM images of Ag NPs on different substrates after sintering under different conditions. All images have the same magnification. a–d): Ag NPs on NB-TP-3GU100 substrates sintered for 64 min. e–h): Ag NPs on Melinex ST506 substrates sintered for 64 min. i–j): Ag NPs on Kapton HN substrates sintered for 4 min in (i) DIW at 85°C, and (j) in the oven at 250°C.

Ag NPs. However, when the substrate temperature during printing is 85°C, there is no significant difference in resistance between samples with or without vacuum drying both before and after water sintering. We assume that after extended periods on the hot plate at 85°C, adsorbed water in the printed Ag tracks is already significantly removed. The vacuum drying process then brings no additional reduction of adsorbed water in the printed Ag tracks but additionally removes the organic solvents.

2.4.2. Thermal Drying

Thermal drying brings no positive influence on water sintering. As shown in **Figure** 7a, after water sintering, the samples in group D dried in an oven at a higher temperature (100°C in this work) have a lower conductivity, while the samples in group A briefly dried on the hot plate (15 min in total including printing and drying) achieve the highest conductivity. This phenomenon can possibly be attributed to cross-linking of capping agent polyvinyl pyrrolidone (PVP). Tan et al. report that below the thermal decomposition temperature of PVP (250°C), the cross-linking rate of PVP is enhanced with increased temperature.[41] Moreover, an interesting effect is the change of color of the samples subjected to these drying processes. The color of the samples in four groups after water sintering is shown in Figure 7b. The samples in group C and D exhibit a brown hue while groups A and B appear more yellowish. To exclude a chemical influence e.g., silver oxide formation, we make energy-dispersive X-ray spectroscopy (EDX) of the samples in four groups. The

Table 1. Resistance of printed Ag tracks on Melinex ST506 substrate undergoing various treatments. Resistance values are measured from five samples in each group.

T	Vacuum dried (40min), stored under RT (3days)	Without vacuum, stored under RT (3days)	Vacuum dried (40min), then 85°C water sintered (16min)	Without vacuum, then 85°C water sintered (16min)
23°C	non-conductive	399.67(33.65)Ω	180.63(32.20)Ω	still wet, non-conductive
55°C	non-conductive	178.60(6.32)Ω	49.86(3.89)Ω	still wet, non-conductive
85°C	269.40(12.93)Ω	289.40(11.80)Ω	27.21(1.83)Ω	26.19(1.38)Ω

[T]:substrate temperature during printing.

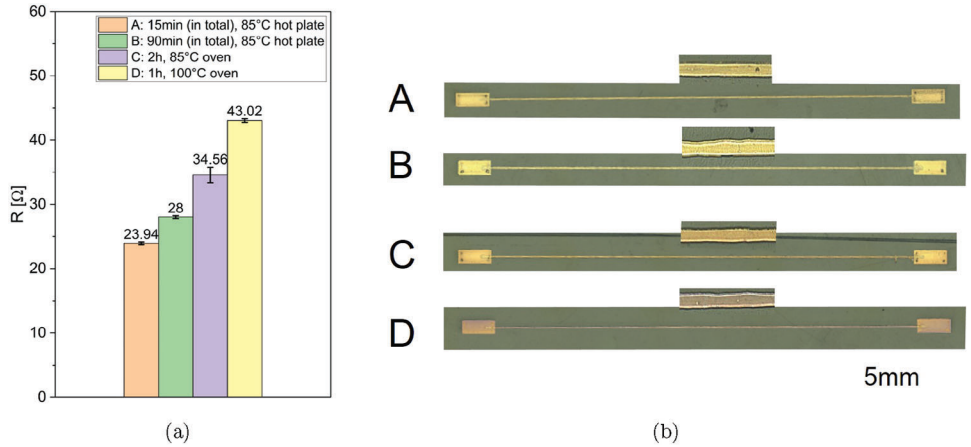

Figure 7. Resistance and color of printed Ag tracks on Melinex ST506 substrate undergoing various thermal drying processes and subsequently 16 min of water watering. For each group, five Ag tracks were printed on a substrate. a) Resistance of the printed Ag tracks after water sintering. b) Color of the printed Ag track in each group after water sintering.

Table 2. Element concentration of printed Ag tracks in four groups.

Group	Drying process	Ag[%]	O[%]	C[%]
A	15 min, 85°C hot plate	95.87	1.16	2.97
B	90 min, 85°C hot plate	95.02	1.18	3.79
C	2 h, 85°C oven	94.23	1.18	4.58
D	1 h, 100°C oven	94.81	1.43	3.76

results in **Table 2** prove that there is no significant difference in the concentration of Ag and oxygen (O_2) between the four groups and also no stoichiometric relation indicating silver oxide formation. On the other hand, the SEM images in **Figure 8** further reveal significant differences in neck formation between Ag NPs in these four groups. These result in different porosities of the water sintered Ag films. As the particle and the pore size are well below the wavelength of light, we assume that the different colors can be attributed to Rayleigh scattering caused by the nanoporous structure.[42] A similar effect has been observed in a nanoporous Ag film created by oxygen plasma.[43] Overall, these findings suggest that thermal drying processes both on the hot plate and in the oven bring no additional benefits but may even negatively impact sintering results.

2.5. Discussion

The above investigation indicates that both damp heat sintering and water sintering yield high conductivity of printed tracks of Ag NP ink (Silverjet DGP 40LT-15C) already at temperatures as low as 85°C. The resulting resistance is only about twice that of thermally sintered Ag NPs at 250°C. In terms of effectiveness, water sintering is found to be more effective than damp heat sintering for the three substrate types studied in this work. Four minutes of water sintering can achieve almost the same effect as 24 h of damp heat sintering at the same temperature of 85°C. Our experiment with silicone oil shows that sintering at these low temperatures is not just due to fluid heat transfer. The other investigations above allow us to explain the sintering mechanism of the Ag NPs at low temperatures. We first look at different states of the capping layer and their influence on other sintering processes.

2.5.1. States of the Capping Layer and their Influence on Standard Sintering Processes

Low molecular weight PVP is usually used in the fabrication of larger nanoparticles as applied in the Ag NP ink.[44] Hereby, increasing with molecular weight, thermal decomposition of PVP starts between 250 and 600°C. Hence, the lower thermal composition temperature of 250°C can be assumed. This is confirmed

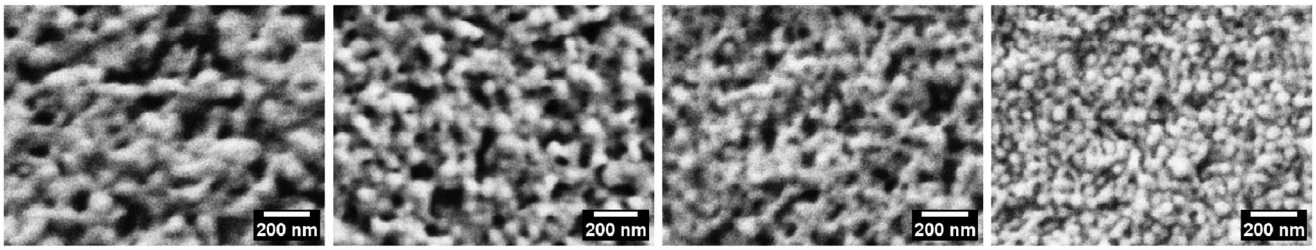

Figure 8. SEM images from Ag NPs after water sintering in a) group A, b) group B, c) group C and d) group D. All SEM images have the same magnification.

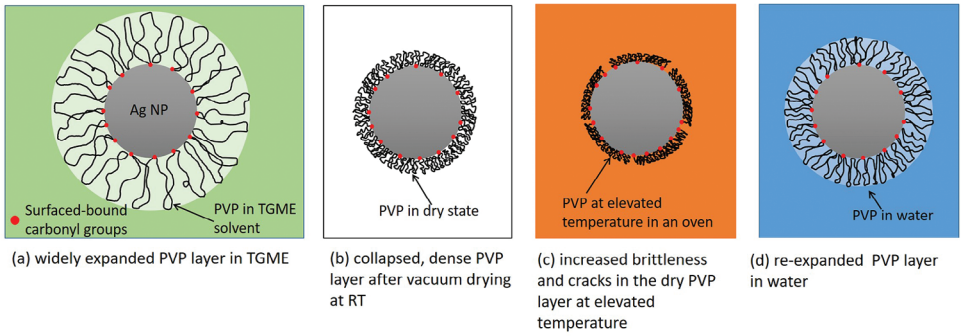

(a) widely expanded PVP layer in TGME

(b) collapsed, dense PVP layer after vacuum drying at RT

(c) increased brittleness and cracks in the dry PVP layer at elevated temperature

(d) re-expanded PVP layer in water

Figure 9. Schematic illustration of a PVP-capping layer in four different states: a) in the solvent TGME, b) after low temperature drying or vacuum drying, c) in an oven at an elevated temperature, and d) in water.

by measurements for PVP-capped Ru-NPs where a decomposition of the PVP capping layer has been observed at 260.98°C.[45] Capping layer decomposition is being used in the high temperature (above 250°C) thermal sintering of Ag NPs on high temperature substrates such as PI films.

Below the decomposition point, the capping layer can assume different states depending on the environmental conditions. **Figure 9** illustrates the PVP capping layer of an Ag NP in four different states: a) in a good solvent, such as triethylene glycol monomethyl ether (TGME), the PVP capping layer is widely expanded and thus keeps the NPs apart;[46] b) when the printed PVP-capped Ag NPs are dried at low temperatures or vacuum dried at RT, the PVP layer collapses and forms a dense layer around the NP; c) below the decomposition point but at elevated temperatures (120–150°C) in an oven, the PVP layer becomes denser, brittle and starts to crack;[47] d) the collapsing of the dried PVP layer is reversible.[46] Hence, when the PVP-capped Ag NPs are subjected to water, the PVP layer can re-expand.

At temperatures beyond the PVP decomposition point, the capping layer is completely removed. However, in the lower thermal temperature sintering range (such as 120–150°C), the cracks in the PVP layer allow metallic contact between the particles and thus lead to sintering (**Figure 10**).

2.5.2. Water Influence on the Properties of the Capping Layer

Apart from the thermal effects outlined above, an aqueous environment also has a significant influence on a PVP capping layer and thus on NP sintering. As shown in **Figure 11**, in a chemical sintering process, the capping layer around the Ag NPs can be removed in an aqueous environment by destabilizing agents such as NaCl.[13] However, in our work, such a chemical destabilization of the capping layer can be excluded, since only DIW is applied for the damp heat and the water sintering process. Moreover, to our knowledge, at least for the Melinex ST506 and Kapton HN substrates, no chemical coating for capping layer destabilization is documented.

Even without destabilizing agents, the remaining factor humidity/water, however, has a strong effect on PVP. Solvent absorption in the PVP capping layer is reversible. This means that after the solvent TGME has evaporated in the drying process and the PVP layer has collapsed, it can re-expand when subjected to another solvent (in our case water, see Figure 9d). Compared to TGME, water is a poor solvent for PVP.[46] However, PVP exhibits a strong hygroscopic effect growing exponentially with humidity.[48] The influence of moisture on the stability of PVP as capping layer has been investigated for pharmaceutical applications.[49] The authors found that already at RT an increase of humidity from 0% to 85% leads to an increase of the weight fraction of water in the polymer to up to 23%. This absorbed water works as a plasticizer for the polymer, lowering its glass transition temperature significantly below 100°C.[49] Moreover, Rhodamin 6G tracer experiments show that at low RH of 30%, the PVP polymer swells slightly. Changing the ambient RH from 60% to 75% results in a sixfold increase in average values of the microdiffusion coefficient for the tracer molecules.[50] Therefore, it can be assumed that in the applied damp heat environment, increased diffusivity of Ag in the aqueous environment and the mechanical properties of the PVP capping layer turn from glassy state to rubbery state. Thus, contact between NPs and neck formation initially due to Ostwald ripening[13] in the aqueous environment can occur. The AFM image of a damp heat sintered sample on Melinex substrate also

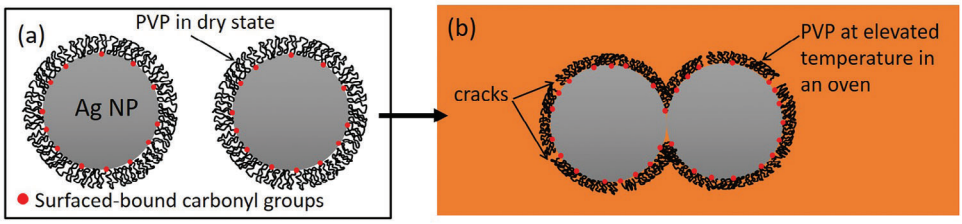

Figure 10. Schematic illustration of thermal sintering mechanism of PVP-capped Ag NPs at temperatures below the decomposition point (such as 120–150°C). a) After drying, the solvent evaporates and the PVP capping layer collapses. b) The cracks in the PVP layer allow metallic contact between the particles, leading to the sintering effect.

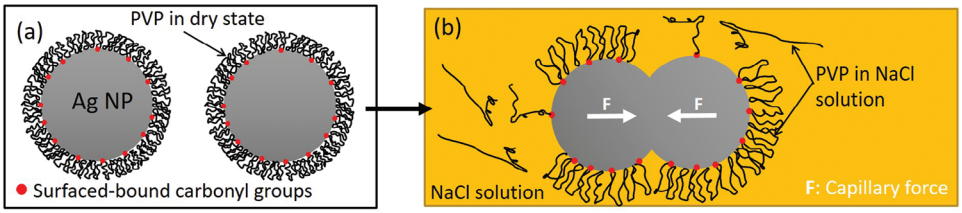

Figure 11. Schematic illustration of the chemical sintering of Ag NPs. a) After drying, the solvent evaporates and the PVP capping layer collapses. b) In an aqueous environment with destabilizing agents (NaCl solution), the PVP capping agent around the Ag NPs can be removed, leading to direct metallic contact and capillary force assisted sintering.

provides evidence of the process of Ostwald ripening (Figure S5, Supporting Information).

2.5.3. Sintering Pressure Arising from Capillary Forces

Substantial capillary forces arise from water menisci between NPs. This effect has already been observed and theoretically studied for sintering processes in metallurgy by Heady et al.[51] For closely packed spheres they estimate an external pressure P_x equivalent to these capillary forces with the following Equation (1), where γ_{LV} is the surface free energy of the liquid-vapor, R is the radius of the spheres, and θ is the contact angle of the liquid-solid-vapor system (θ is measured "in" the liquid).[51]

$$P_x = 2\sqrt{2}\pi(\gamma_{LV}/R)cos\theta \quad (1)$$

As the capping agent PVP has a hydrophilic endgroup,[49] we assume full wetting of the silver particles by the water film, i.e., set θ= 0°, R = 25nm. Moreover, we neglect the influence of the water-soluble ink solvent TGME residue on the surface energy of water. We take into account the temperature-dependent surface energy values of water calculated with the calculator at the website of the International Association for the Properties of Water and Steam.[52] Under these assumptions, calculation of the equivalent external pressure P_x with Equation (1) yields 25.7MPa for 23°C, 23.8MPa for 55°C and 21.9MPa for 85°C. This means, capillary pressure declines from 23 to 85°C by about 15 % due to the temperature-dependent decline of the surface energy of water. But even the lower value still yields a substantial equivalent external pressure that will definitely contribute to nanoparticle sintering.

Figure 12 schematically illustrates the damp heat/water sintering mechanism. After drying, the solvent TGME evaporates and the PVP capping layer collapses. When dried PVP-capped Ag NPs are subjected to a damp heat environment or immersed in hot water, the PVP capping layer re-expands and turns from a glassy state to a rubbery state, which facilitates the Ag diffusion in the Ostwald ripening process. Meanwhile, the capillary pressure arising from water menisci provides an additional mechanical pressure to the sintering process. Neck formation between Ag NPs occurs and increases the conductive paths, leading to a substantial decrease in resistance already at temperatures significantly below the thermal sintering range.

The sensitivity of PVP against moisture also explains why water sintering is even more effective than damp heat sintering, since full immersion in water should lead to even more depression of the PVP glass transition temperature and more diffusivity of the PVP layer, yielding it even more permeable and the capillary pressure more effective. Full immersion of the sample in water results in neck formation of Ag NPs within minutes compared to hours in damp heat sintering. While water sintering is a simple process and requires no extra equipment other than a hot plate and a thermal sensor to control the temperature of the water, its disadvantage can be the delamination of the printed structures from the substrate. We observe delamination between the Ag layer and the Kapton HN substrate after four minutes of water sintering, while even after 24 h of damp heat sintering, this problem is not observed.

3. Conclusion

In this work, we have systematically conducted experiments to investigate the influence of damp heat and hot water treatment on structures printed with Ag NP ink (Silverjet DGP 40LT-15C)

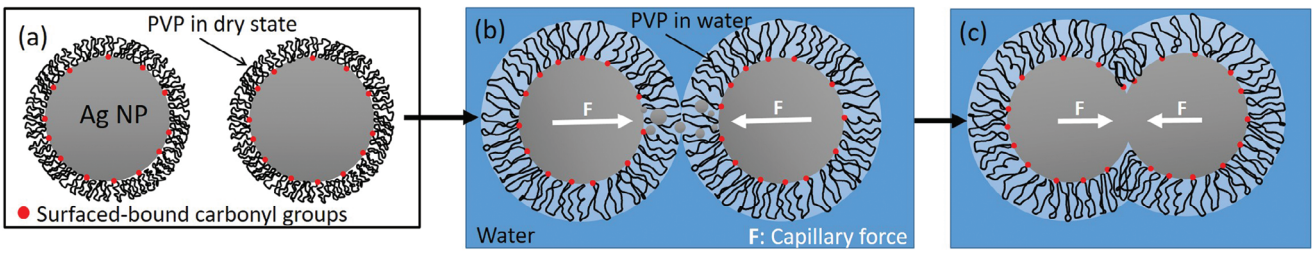

Figure 12. Schematic illustration of the damp heat/water sintering of Ag NPs. a) After drying, the solvent evaporates and the PVP capping layer collapses. b) Subjecting the dried PVP-capped Ag NPs to a damp heat environment or hot water, the PVP capping layer expands and turns from a glassy state to a rubbery state, which facilitates the Ag diffusion in the Ostwald ripening process. Meanwhile, the capillary pressure arising from water menisci yields an additional force contributing to the sintering of Ag NPs. c) Neck formation between Ag NPs occurs.

onto three different substrates. We find that both damp heat and immersion in hot water, at temperatures up to 85°C lead to neck formation between Ag NPs and thus, to sintering effects already in low temperature ranges. While both, a damp heat and a hot water process, exhibit good sintering effects, they also have their pros and cons. Immersion in hot water achieves low resistances within minutes while achieving similar resistances in a damp heat atmosphere takes up to 24 h. On the other hand, immersion in hot water can lead to delamination of the printed Ag NP structure from the PI substrate, destroying the structure. Measures can be taken to prevent delamination. E.g., Olkkonen et al. find that an adhesion enhancement can be achieved by UV pretreatment.[36] This adhesion problem was not observed in the damp heat process. After 24 h of damp heat sintering, the resistivity of printed tracks is 5.16μΩcm, which is only 1.7 times that of the printed Ag tracks thermally sintered at 250°C. Further experiments were performed to differentiate the influence of heat and water. We assume that neck formation between nanoparticles results from a combination of a humidity dependent reduction of the glass transition temperature of the PVP capping layer, leading to higher diffusivity of the capping layer and subsequently to Ostwald ripening, and capillary pressure arising from water menisci between nanoparticles. The capillary pressure is a general influence resulting from the high surface energy of water and is mainly dependent on the wetting properties of the nanoparticles with their capping layer. The reduction of the glass transition temperature and the associated increase of diffusivity is, however, specific to the capping layer material.

Compared to thermal sintering at the temperature range of 120–150°C, the damp heat/water sintering processes investigated in this work can be conducted at a low temperature of 85°C and achieve good conductivity of the printed Ag tracks. Chemical sintering in an aqueous environment with destabilizing agents such as Cl^- ions can weaken the adhesion between printed structure and substrate since the capping layer is removed by destabilizing agents, while the capping layer is reported essential for this adhesion.[36] This adhesion problem was not observed in the damp heat sintering process in this work since rather than the removal of the capping layer, our damp heat sintering process results in softening and increased diffusivity of the capping layer.

Our experiments indicate that with the humid atmosphere established in the chamber, the damp heat sintering is an efficient sintering process in particular for low temperature substrates such as PET. A plausible application could involve incorporating a damp heat sintering chamber into a roll-to-roll production line, where the substrate slowly passes through and gets sintered in transfer. In principle, such an approach could also be considered for the water sintering process, provided the delamination problem does not occur or has been resolved as outlined by Olkkonen et al.[36]

In the case of the Ag NP ink used in these investigations, this capping layer is PVP. Hence, in order to decide if damp heat and possibly, depending on the substrate, hot water immersion are indeed alternative low temperature sintering processes, further investigations are required. In a first step, experiments with other metal NP inks with the same capping agent such as gold nanoparticle inks[53–55] have to be conducted to find out if these sintering processes are applicable to this class of inks. In a second step, metal NP inks with polymer other capping agents (e.g., PVA) should be investigated to see if similar influences of humidity on these respective capping agents can be observed that also lead to neck formation in the low-temperature range. If these effects can be indeed confirmed for a broad scope of metal NP inks, low-temperature damp heat, and hot water processing can become alternative, effective, low-cost, and low-temperature sintering methods.

4. Experimental Section

Materials: The Ag NP ink (Silverjet DGP 40LT-15C) was purchased from Sigma–Aldrich. This ink consists of 30–35wt.% Ag NP in the solvent TGME. According to earlier studies,[56,57] PVP was applied as capping agent for this ink. The recommended sintering temperature was 100–150°C. The data sheet of this ink provides a specific resistivity of 11μΩcm after sintering at 250°C for three hours. PET films (Mitsubishi NB-TP-3GU100, 138μm thickness[40]; DuPont Teijin Films Melinex ST506, 175μm thickness) were used as substrates. NB-TP-3GU100 films show significant deformations at temperatures above 100°C due to the nanoporous coating on one surface. Melinex ST506 were heat stabilized PET films for withstanding processing temperatures of up to 150°C,[58] possessing an acrylic pretreatment on both surfaces to enhance adhesion to inks.[59] Another type of film used as a substrate is PI (Kapton HN, DuPont, 75μm thickness). Kapton HN films were known as high-temperature substrates and could be heated up to about 400°C. Silicone oil for the oil bath was purchased from VWR Chemicals (VWR catalog number: 24610.363).

Test Structure: The length of the designed Ag tracks was 45mm. The pads at both ends of the Ag tracks were 1.5mm × 3.5mm. The drop distance was set to 50μm on NB-TP-3GU100, and 100μm on Melinex ST506 and Kapton HN. The Ag tracks were printed in two passes.

Inkjet Printing: An Autodrop Gantry inkjet printer with a MD-K-140 single nozzle piezo printhead (nozzle diameter: 50μm) from Microdrop Technologies GmbH was utilized for printing the Ag tracks. The printing parameters, including voltage, and pulse width, were set to 170V and 45μs, respectively. A vacuum of -7mbar was applied on the ink vessel. For the experiments in Sections 2.2 and 2.3, the Ag tracks were printed on NB-TP-3GU100 substrates at RT and left to dry for seven days at RT. In order to reduce the spreading of the ink, when Melinex ST506 and Kapton HN were used as substrates, the temperature of the printer hotplate was set to 85°C during printing. Five Ag tracks were printed as a group and eight groups of Ag tracks were printed on one substrate. The printing time on one substrate was about 60 min. After printing, the samples were left for drying on the printer hot plate at 85°C for additional 45 min.

Damp Heat Sintering: Damp heat sintering was conducted in a climate chamber (Memmert CTC 256). The test conditions were set to 85%RH and three different temperatures, 23, 55, and 85°C (Figure S3, Supporting Informtion). Three to five samples were sintered for every temperature. The resistance of the printed samples was measured before sintering and after one hour, three hours, and 24 hours of sintering. The detailed settings of damp heat sintering tests were listed in Table S2 (Supporting Information). To compare the results to the thermal sintering process, reference samples were thermally sintered in a convection oven (Memmert UF30 plus). The thermal sintering temperatures were set to 85°C for the printed samples on NB-TP-3GU100 and Melinex ST506 substrates, and 250°C for those on Kapton HN substrates.

Water Sintering: To maximize the exposure of the samples to water at different temperatures, the printed Ag tracks were immersed in DIW at different temperatures (Figure S6 and Table S3, Supporting Information). Four-point resistance measurements were taken before and after each immersion.

Separation of Physical and Chemical Influences of Water: As water was a substance with very special chemical (e.g., highly polar) and physical properties (e.g., high surface energy, high heat capacity), these chemical and physical influences were analyzed separately. A possible reason for the observed sintering effect could be physical, i.e., more intensive heat

transfer by a fluid phase with high heat capacity. In order to investigate the influence of a more intensive heat transfer, reference samples on NB-TP-3GU100 and Melinex ST506 PET substrates were immersed in a water-free fluid, a silicone oil bath at 85°C for the same durations as for the water sintering process.

Vacuum Drying: Samples were printed on Melinex ST506 substrates at three different temperatures (23, 55, and 85°C) and stayed on the hot plate for 15 min in total. In order to remove ink solvents, they were then subjected to a vacuum drying for 40 min at a pressure of 0.3mbar in the chamber of a plasma oven (Diener Atto) and electrically characterized followed by 16 min of water sintering (Figure S8, Supporting Information).

Thermal Drying: To investigate whether a thermal drying process brings potential impact on the subsequent water sintering process, additional samples were printed on Melinex ST506 substrates. During the printing process, the temperature of the hot plate was 85°C and samples stayed on the hot plate for 15 min in total. After that, the samples in group A were directly immersed into DIW at 85°C for 16 min. The samples in group C were placed in the oven at 85°C for two hours, and the samples in group D in the oven at 100°C for one hour before immersion in DIW at 85°C for 16 min. The experimental setup is shown in Figure S9 (Supporting Information). To compare, the samples in group B are taken from Section 2.3, and they stayed on the printer hot plate at 85°C for 90 min in total before immersion in DIW at 85°C for 16 min.

Characterization: The length of printed Ag NP tracks was measured using a Keyence VHX 7000 microscope. The width, the profile area of printed silver tracks, and the roughness of three types of substrates were measured using a MahrSurf CM select confocal microscopy. The obtained data was analyzed using MountainsLab software. SEM images were taken from the top of silver tracks using a Zeiss SUPRA 60 VP. EDX analysis was conducted using an Ultim Extreme silicon drift detector (Oxford Instruments, AZtec software) at a SEM (Zeiss SUPRA 55) acceleration voltage of 4kV to determine the elemental composition. Four-point resistance measurements were conducted using a B&K Precision LCR-Meter 981 connected to a Formfactor EPS150 probestation with probe tip size of 150µm.

Statistical Analysis: In Section 2.1, three Ag tracks on each substrate, and five profiles (with a 10mm spacing between each profile) on each Ag track were measured. The obtained profile data was analyzed using MountainsLab software and the data presentation was (mean ± SD). For each damp heat and water sintering experiment in Sections 2.2 and 2.3, three to five samples were analyzed. For each experiment in Section 2.4, five samples were analyzed and the data presentation was (mean ± SD) in Table 1. One sample in each group in Table 2 was analyzed for EDX analysis. Statistical analysis of graph data was plotted using OriginLab software.

Supporting Information

Supporting Information is available from the Wiley Online Library or from the author.

Acknowledgements

This work was funded by the program Material Systems Engineering of the Helmholtz Association.

Open access funding enabled and organized by Projekt DEAL.

Conflict of Interest

The authors declare no conflict of interest.

Data Availability Statement

The data that support the findings of this study are available from the corresponding author upon reasonable request.

Keywords

capping agent, inkjet printing, low-temperature sintering, neck formation, printed electronics, silver nanoparticle

Received: August 10, 2023
Revised: November 28, 2023
Published online:

[1] L.-W. Lo, H. Shi, H. Wan, Z. Xu, X. Tan, C. Wang, *Adv. Mater. Technol.* **2019**, *5*, 1900717.
[2] J. Zikulnig, C. Hirschl, L. Rauter, M. Krivec, H. Lammer, F. Riemelmoser, A. Roshanghias, *Flexible Printed Electron.* **2019**, *4*, 015008.
[3] S. K. Karunakaran, G. M. Arumugam, W. Yang, S. Ge, S. N. Khan, X. Lin, G. Yang, *J. Mater. Chem. A* **2019**, *7*, 13873.
[4] P. G. V. Sampaio, M. O. A. González, P. O. Ferreira, P. C. J. Vidal, J. P. P. Pereira, H. R. Ferreira, P. C. Oprime, *Int. J. Energy Res.* **2020**, *44*, 9912.
[5] M. Hengge, K. Livanov, N. Zamoshchik, F. Hermerschmidt, E. J. W. List-Kratochvil, *Flexible Printed Electron.* **2021**, *6*, 015009.
[6] Y. Murat, K. Petersons, D. Lanka, L. Lindvold, L. Yde, J. Stensborg, M. Gerken, *Mater. Adv.* **2020**, *1*, 2755.
[7] X. Du, S. P. Wankhede, S. Prasad, A. Shehri, J. Morse, N. Lakal, *J. Mater. Chem. C* **2022**, *10*, 14091.
[8] U. Gengenbach, M. Ungerer, L. Koker, K.-M. Reichert, P. Stiller, S. Allgeier, B. Köhler, X. Zhu, C. Huang, V. Hagenmeyer, *Mechatronics* **2020**, *70*, 102403.
[9] M. Ungerer, Dissertation, Karlsruhe Institute of Technology, Karlsruhe, **2020**.
[10] A. Sharif, J. Ouyang, A. Raza, M. A. Imran, Q. H. Abbasi, *Microwave Opt. Tech. Lett.* **2019**, *61*, 2161.
[11] V. K. R. Rao, A. K. Venkata, P. S. Karthik, S. P. Singh, *RSC Adv.* **2015**, *5*, 77760.
[12] Q. Huang, Y. Zhu, *Adv. Mater. Technol.* **2019**, *4*, 1800546.
[13] L. Mo, Z. Guo, L. Yang, Q. Zhang, Y. Fang, Z. Xin, Z. Chen, K. Hu, L. Han, L. Li, *Int. J. Mol. Sci.* **2019**, *20*, 2124.
[14] K.-S. Chou, K.-C. Huang, H.-H. Lee, *Nanotechnology* **2005**, *16*, 779.
[15] J. R. Greer, R. A. Street, *Acta Mater.* **2007**, *55*, 6345.
[16] W. Luo, W. Hu, S. Xiao, *J. Phys. Chem. C* **2008**, *112*, 2359.
[17] A. Denneulin, A. Blayo, C. Neuman, J. Bras, *J. Nanopart. Res.* **2011**, *13*, 3815.
[18] J. S. Kang, J. Ryu, H. S. Kim, H. T. Hahn, *J. Electron. Mater.* **2011**, *40*, 2268.
[19] Y.-R. Jang, S.-J. Joo, J.-H. Chu, H.-J. Uhm, J.-W. Park, C.-H. Ryu, M.-H. Yu, H.-S. Kim, *Int. J. Prec. Eng. Manuf.-Green Tech.* **2020**, *8*, 327.
[20] A. Chiolerio, G. Maccioni, P. Martino, M. Cotto, P. Pandolfi, P. Rivolo, S. Ferrero, L. Scaltrito, *Microelectron. Eng.* **2011**, *88*, 2481.
[21] O. Ermak, M. Zenou, G. B. Toker, J. Ankri, Y. Shacham-Diamand, Z. Kotler, *Nanotechnology* **2016**, *27*, 385201.
[22] W. Gu, W. Yuan, T. Zhong, X. Wu, C. Zhou, J. Lin, Z. Cui, *RSC Adv.* **2018**, *8*, 30215.
[23] B. J. Perelaer, A. W. M. de Laat, C. E. Hendriks, U. S. Schubert, *J. Mater. Chem.* **2008**, *18*, 3209.
[24] M. J. Renn, M. Schrandt, J. Renn, J. Q. Feng, *J. Microelectron. Electron. Packag.* **2017**, *14*, 132.
[25] X. Zhao, Z. Deng, W. Zhao, B. Feng, M. Wang, M. Huang, L. Liu, G. Zou, Y. Shao, H. Zhu, *Nanoscale* **2020**, *12*, 19413.
[26] I. Lee, A. Hussain, H.-L. Lee, Y.-J. Moon, J.-Y. Hwang, S.-J. Moon, *Metals* **2021**, *11*, 1878.
[27] M. Allen, A. Alastalo, M. Suhonen, T. Mattila, J. Leppaniemi, H. Seppa, *IEEE Trans. Microwave Theory Tech.* **2011**, *59*, 1419.

[28] J. Perelaer, B.-J. de Gans, U. Schubert, *Adv. Mater.* **2006**, *18*, 2101.
[29] D. Corzo, G. Tostado-Blázquez, D. Baran, *Front. Electron.* **2020**, *1*, 594003.
[30] V. Zardetto, T. M. Brown, A. Reale, A. Di Carlo, *J. Polym. Sci., Part B: Polym. Phys.* **2011**, *49*, 638.
[31] S. Magdassi, M. Grouchko, O. Berezin, A. Kamyshny, *ACS Nano* **2010**, *4*, 1943.
[32] Y. Tang, W. He, G. Zhou, S. Wang, X. Yang, Z. Tao, J. Zhou, *Nanotechnology* **2012**, *23*, 355304.
[33] D. C. Corsino, M. D. L. Balela, *IOP Conf. Ser.: Mater. Sci. Eng.* **2017**, *264*, 012020.
[34] P. Peng, L. Li, W. Guo, Z. Hui, J. Fu, C. Jin, Y. Liu, Y. Zhu, *J. Phys. Chem. C* **2018**, *122*, 2704.
[35] Y. Xiao, Z. Zhang, M. Yang, H. Yang, M. Li, Y. Cao, *Mater. Lett.* **2018**, *222*, 16.
[36] J. Olkkonen, J. Leppäniemi, T. Mattila, K. Eiroma, *J. Mater. Chem. C* **2014**, *2*, 3577.
[37] Y. Yang, S. Duan, H. Zhao, *Nanoscale* **2022**, *14*, 11484.
[38] J. Bourassa, A. Ramm, J. Q. Feng, M. J. Renn, *SN Appl. Sci.* **2019**, *1*, 6.
[39] M. Allen, J. Leppäniemi, M. Vilkman, A. Alastalo, T. Mattila, *Nanotechnology* **2010**, *21*, 475204.
[40] M. Ungerer, W. Spomer, I. Wacker, R. Schröder, U. Gengenbach, *Int. J. Adv. Intell. Syst.* **2017**, *10*, 383.
[41] L. Tan, X. Zheng, L. Chen, Y. Wang, *J. Sep. Sci.* **2014**, *37*, 2974.
[42] K. Li, C. Li, H. Li, M. Li, Y. Song, *iScience* **2021**, *24*, 102121.
[43] C. Ma, M. J. Trujillo, J. P. Camden, *ACS Appl. Mater. Interfaces* **2016**, *8*, 23978.
[44] A. Rónavári, P. Bélteky, E. Boka, D. Zakupszky, N. Igaz, B. Szerencsés, I. Pfeiffer, Z. Kónya, M. Kiricsi, *Int. J. Mol. Sci.* **2021**, *22*, 8673.
[45] M. Kumar, P. Devi, V. D. Shivling, *Mater. Res. Express* **2017**, *4*, 085006.
[46] T.-H. Yang, J. Ahn, S. Shi, D. Qin, *ACS Nano* **2021**, *15*, 14242.
[47] A. Jarray, V. Gerbaud, M. Hemati, *Prog. Org. Coat.* **2016**, *101*, 195.
[48] F. Haaf, A. Sanner, F. Straub, *Polym. J.* **1985**, *17*, 143.
[49] S. Fitzpatrick, J. F. McCabe, C. R. Petts, S. W. Booth, *Int. J. Pharm.* **2002**, *246*, 143.
[50] S. Bhattacharya, D. K. Sharma, S. Saurabh, S. De, A. Sain, A. Nandi, A. Chowdhury, *J. Phys. Chem. B* **2013**, *117*, 7771.
[51] R. B. Heady, J. W. Cahn, *Metall. Trans.* **1970**, *1*, 1.
[52] The international association for the properties of water and steam (iapws), http://www.iapws.org/ (accessed: April 2023).
[53] W. Cui, W. Lu, Y. Zhang, G. Lin, T. Wei, L. Jiang, *Colloids Surf. A* **2010**, *358*, 35.
[54] H. R. Tiyyagura, P. Majerič, M. Bračič, I. Anžel, R. Rudolf, *Nanomaterials* **2021**, *11*, 599.
[55] W. Li, Q. Cen, W. Li, Z. Zhao, W. Yang, Y. Li, M. Chen, G. Yang, J. Yang, *J. Mater.* **2020**, *6*, 300.
[56] H. Andersson, A. Manuilskiy, T. Unander, C. Lidenmark, S. Forsberg, H.-E. Nilsson, *IEEE Sens. J.* **2012**, *12*, 1901.
[57] S. Kim, S. Won, G.-D. Sim, I. Park, S.-B. Lee, *Nanotechnology* **2013**, *24*, 085701.
[58] W. A. MacDonald, R. Eveson, D. MacKerron, R. Adam, K. Rollins, R. Rustin, M. K. Looney, J. Stewart, K. Hashimoto, *SID Symp. Digest Tech. Papers* **2007**, *38*, 373.
[59] J. Smith, R. Hamilton, I. McCulloch, M. Heeney, J. E. Anthony, D. D. Bradley, T. D. Anthopoulos, *Synth. Met.* **2009**, *159*, 2365.